Entanglement skyrmions in multicomponent quantum Hall systems

B. Douçot,[1] M. O. Goerbig,[2] P. Lederer,[2] and R. Moessner[3]
[1]*Laboratoire de Physique Théorique et Hautes Energies, CNRS UMR 7589, Université Paris 6 et 7, F-75252 Paris Cedex, France*
[2]*Laboratoire de Physique des Solides, CNRS UMR 8502, Université Paris Sud , F-91405 Orsay Cedex, France*
[3]*Max-Planck-Institut für Physik Komplexer Systeme, 01187 Dresden, Germany*
(Received 7 June 2008; revised manuscript received 3 October 2008; published 26 November 2008)

We discuss charged topological spin textures in quantum Hall ferromagnets in which the electrons carry a pseudospin, as well as the usual spin degree of freedom, as is the case in bilayer GaAs or monolayer graphene samples. We develop a theory which treats spin and pseudospin on a manifestly equal footing, which may also be of help in visualizing the relevant spin textures. We in particular consider the entanglement of spin and pseudospin in the presence of realistic anisotropies. An entanglement operator is introduced, which generates families of degenerate skyrmions with differing entanglement properties. We propose a local characterization of the latter and touch on the role entangled skyrmions play in the nuclear relaxation time of quantum Hall ferromagnets.

DOI: 10.1103/PhysRevB.78.195327 PACS number(s): 73.43.Lp, 73.21.−b, 81.05.Uw

I. INTRODUCTION

Quantum Hall (QH) systems with supplementary degrees of freedom are fascinating objects of study, exhibiting phenomena such as the superfluid behavior in quantum Hall bilayers at total filling factor $\nu=1$.[1–9] In those systems, the superfluid ground state is isomorphous to a quantum Hall monolayer ferromagnetic ground state at the same filling factor, but in terms of the $S=1/2$ pseudospin degree of freedom encoding which layer an electron finds itself in. A similar pseudospin ferromagnet is surmised to occur in a graphene monolayer, where the pseudospin degree of freedom is analogously connected to the two degenerate midband valleys.[10–12]

In quantum Hall ferromagnets at $\nu=1$, the lowest charged excited states are topological defects, called skyrmions,[13] which in turn are fascinating in their own right. Indeed they are spin textures carrying a topological quantum number and which necessarily carry a quantized net charge. The properties of skyrmions in QH physics have been studied extensively since their theoretical prediction[14] and experimental confirmation[15] in the mid-1990s. These charged topological spin textures are due to the strong electronic correlations once the low-energy excitations are restricted to a single Landau level (LL). They can exist as quasiparticles of a ferromagnetic ground state near a LL filling factor $\nu=1$, where $\nu=n_{\mathrm{el}}/n_B$ is the ratio between electronic density n_{el} and $n_B=eB/h=1/2\pi l_B^2$ that of the flux quanta h/e threading an area of the two-dimensional (2D) electron gas at a particular magnetic field B (here, $l_B=\sqrt{\hbar/eB}$ is the magnetic length).

In bilayer QH systems, in contrast to the intrinsic electronic spin 1/2 in monolayer QH systems, the effective interaction becomes pseudospin dependent due to the different interaction strength between electrons in the same layer and that of between particles in different layers.[16,17] It is indeed energetically unfavorable to have all electrons in the same layer because of a finite amount of charging energy per particle. This results in an easy-plane ferromagnetic ground state, i.e., in which the pseudospin magnetization is constrained in the xy plane. Bilayer ferromagnets have, thus, an easy-plane [U(1)] symmetry.

Topological excitations of easy-plane ferromagnets in bilayer QH systems are conventionally described in terms of merons classified by their charge $(\pm 1/2)$ and their vorticity (± 1).[16] As each meron has a logarithmically divergent energy, one needs two merons with opposite vorticity to make a topologically stable excitation of finite energy (bimeron), which may also be viewed as a pseudospin skyrmion.

Besides the physical spin in monolayer and the layer pseudospin in bilayer QH systems, valley indices can be encoded by pseudospin degrees of freedom. The indirect-gap semiconductors Si and AlAs are well-studied instance,[18,19] as is the pair of Dirac points in graphene.[20]

One particularly interesting situation arises when the internal Hilbert space comprises both the spin and the additional pseudospin. This combination can in principle lead to an internal space with a high symmetry, such as SU(4) for a combination of a spin and pseudospin pair of SU(2)'s. The properties of SU(4) skyrmions were considered by Ezawa[21] and that of general SU(N) skyrmions for $N>2$ by Arovas *et al.*[22] SU(4) skyrmions have recently been revisited by Yang *et al.*[23] in the context of graphene.

However, the Hamiltonian generically contains anisotropy terms violating the full symmetry. In the simplest situation of a Zeeman field, the symmetry $\sigma^z \leftrightarrow -\sigma^z$ is removed. Such symmetry-breaking terms can in principle also be manipulated, for example the effective g factor determining the strength of the Zeeman coupling can be tuned by applying external pressure thanks to spin-orbit coupling. The energetics of the resulting topological excitations has been an active field of study in recent years.[24–30]

In this paper, we consider the properties of SU(2) $\times$ SU(2) skyrmions in the presence of realistic anisotropy terms. We do this from a perspective of entanglement between the spin and pseudospin degrees of freedom. As our point of departure, we parametrize the general SU(4) skyrmion using a Schmidt decomposition.[31] Our parametrization is manifestly symmetric between the two SU(2) copies aris-

ing from spin and pseudospin. In addition, a third ("entanglement") spinor appears. These features turn out to be of help in visualizing the nature of different types of SU(4) skyrmions, for instance by providing a simple picture for the relative entanglement between spin and pseudospin.

With this in hand, we compute the Berry connection and then display in a transparent way the properties of entanglement textures. [The topological stability of the SU(4) skyrmion becomes, strictly speaking, apparent only in the associated CP^3 description.] Crucially, we show that there exist entire U(1) families of degenerate skyrmions which differ by their degree of entanglement.

This in particular leads to the distinction of two different topological excitations, both of which have zero expectation value of transverse spin but in only one of which the spin degree of freedom is involved. At some special "maximally entangled" points, the "order parameters" $\langle\vec{\sigma}\rangle$ and $\langle\vec{\tau}\rangle$ may even vanish altogether.

This treatment offers some further insights into the magnetic properties of multicomponent systems, which have been studied experimentally in recent years, in the framework of nuclear magnetic resonance (NMR) experiments on bilayer QH systems.[32,33] In particular, we briefly discuss how entangled excitations affect the spin degrees of freedom measured in NMR experiments.

The paper is organized as follows. In Sec. II, we introduce the basic model and the parametrization of the spin-pseudospin degrees of freedom. Spin-pseudospin entanglement is studied in Sec. III, where we propose a measure of such entanglement, the properties of which are described in Sec. IV. Section V reviews the relevant energy scales of bilayer and graphene QH systems, where entanglement skyrmions may be physically relevant. The dynamical properties of entangled spin-pseudospin textures and their consequences for NMR measurements are discussed in Sec. VI.

II. MODEL AND PARAMETRIZATION

We study a two-dimensional electron system (2DES) in the QH regime, where the kinetic energy is quenched. We consider two internal degrees of freedom which provide the multicomponent nature of the 2DES: first, the spin degree of freedom, represented by the Pauli matrices σ^a, where $a=x,y,z$; second, the pseudospin, represented by a second set of Pauli matrices, τ^μ, with $\mu=x,y,z$. For concreteness, it may help to have the bilayer index in mind when considering the pseudospin.

A. Parametrization

One may typically describe a texture at overall filling factor $\nu=1$ by a Hartree-Fock state of the form

$$|\Phi\rangle = \prod_X [w_1(X)c^+_{X\uparrow,t} + w_2(X)c^+_{X\uparrow,b} + w_3(X)c^+_{X\downarrow,t} + w_4(X)c^+_{X\downarrow,b}|0\rangle], \quad (1)$$

where X labels orbital states in the plane restricted to the lowest LL. Internal states are labeled according to the projection of the spin along the external magnetic field ($\uparrow$ or $\downarrow$) and the layer (t or b). We assume that the orbital states are each fairly well localized (on a typical scale given by the magnetic length) and mutually orthogonal. The explicit construction of such a basis for any Landau level is given for instance in Ref. 34 and has been used to describe the bilayer system by a lattice SU(4) model.[35] With such a choice, $X \equiv \mathbf{r}$ can be viewed as the location of the center of a given Wannier orbital on a von Neumann lattice. We will always assume that the texture varies slowly on the scale of the magnetic length so that w_i $(1\leq i\leq 4)$ may be regarded as smooth complex functions of a continuous position variable. We will also assume these local four-component spinors to be normalized, that is, $\Sigma_{i=1}^4 |w_i(\mathbf{r})|^2=1$. To get a more direct physical interpretation of such a texture, it is rather natural to express the internal state at site $\mathbf{r}$ in a way that treats both spin and pseudospin degrees of freedom on an equal footing. This is achieved by the Schmidt decomposition[31]

$$|\Psi(\mathbf{r})\rangle = \cos\frac{\alpha}{2}|\psi_S\rangle|\psi_I\rangle + \sin\frac{\alpha}{2}e^{i\beta}|\chi_S\rangle|\chi_I\rangle, \quad (2)$$

where α and β are functions of $\mathbf{r}$, and the local two-component spinors $|\psi_S\rangle$, $|\chi_S\rangle$, $|\psi_I\rangle$, and $|\chi_I\rangle$ are constructed according to

$$|\psi\rangle = \begin{pmatrix} \cos\frac{\theta}{2} \\ \sin\frac{\theta}{2}e^{i\phi} \end{pmatrix}, \quad (3)$$

$$|\chi\rangle = \begin{pmatrix} -\sin\frac{\theta}{2}e^{-i\phi} \\ \cos\frac{\theta}{2} \end{pmatrix}. \quad (4)$$

Here, θ and ϕ are the usual polar angles defining a vector

$$\mathbf{n}(\theta,\phi) = (\sin\theta\cos\phi, \sin\theta\sin\phi, \cos\theta). \quad (5)$$

We will denote the pair for spin (pseudospin) by θ_S,ϕ_S (θ_I,ϕ_I), respectively. Note that the above parametrization for the two-component spinors is not unique because for a given classical unit vector $\mathbf{n}(\theta,\phi)$, we can multiply both $|\psi\rangle$ and $|\chi\rangle$ by global phases that may depend on $\mathbf{r}$. We have chosen the parametrization in order to minimize the occurrence of phase singularities—they appear only when one of the angles θ_S, θ_I, or β is equal to π.

With these notations, the general four-component local spinor [Eq. (2)] has the form

$$|\Psi(\mathbf{r})\rangle = \begin{pmatrix} w_1 \\ w_2 \\ w_3 \\ w_4 \end{pmatrix} = \begin{pmatrix} \cos\frac{\theta_S}{2}\cos\frac{\theta_I}{2}\cos\frac{\alpha}{2} & + \sin\frac{\theta_S}{2}\sin\frac{\theta_I}{2}\sin\frac{\alpha}{2}e^{i(\beta-\phi_S-\phi_I)} \\ \cos\frac{\theta_S}{2}\sin\frac{\theta_I}{2}\cos\frac{\alpha}{2}e^{i\phi_I} & - \sin\frac{\theta_S}{2}\cos\frac{\theta_I}{2}\sin\frac{\alpha}{2}e^{i(\beta-\phi_S)} \\ \sin\frac{\theta_S}{2}\cos\frac{\theta_I}{2}\cos\frac{\alpha}{2}e^{i\phi_S} & - \cos\frac{\theta_S}{2}\sin\frac{\theta_I}{2}\sin\frac{\alpha}{2}e^{i(\beta-\phi_I)} \\ \sin\frac{\theta_S}{2}\sin\frac{\theta_I}{2}\cos\frac{\alpha}{2}e^{i(\phi_I+\phi_S)} & + \cos\frac{\theta_S}{2}\cos\frac{\theta_I}{2}\sin\frac{\alpha}{2}e^{i\beta} \end{pmatrix}. \tag{6}$$

We thus have six parameters $(\theta_S, \phi_S, \theta_I, \phi_I, \alpha, \beta)$, as expected for four complex components minus a global phase and the overall normalization. All of these can vary as functions of the spatial coordinate $\mathbf{r}=(x,y)$ in the xy plane.

The great advantage of factorizing the wave function in such a manner is that we can read off directly the reduced density matrices for the spin and pseudospin sectors,

$$\rho_S = \mathrm{Tr}_I(|\psi\rangle\langle\psi|) = \cos^2\frac{\alpha}{2}|\psi_S\rangle\langle\psi_S| + \sin^2\frac{\alpha}{2}|\chi_S\rangle\langle\chi_S|,$$

$$\rho_I = \mathrm{Tr}_S(|\psi\rangle\langle\psi|) = \cos^2\frac{\alpha}{2}|\psi_I\rangle\langle\psi_I| + \sin^2\frac{\alpha}{2}|\chi_I\rangle\langle\chi_I|$$

for the spin and the pseudospin, respectively. This yields

$$m_S^a = \mathrm{Tr}(\rho_S S^a) = \cos\,\alpha\langle\psi_S|S^a|\psi_S\rangle = \cos\,\alpha n^a(\theta_S,\phi_S) \tag{7}$$

for the local spin and

$$m_I^\mu = \mathrm{Tr}(\rho_I P^\mu) = \cos\,\alpha\langle\psi_I|P^\mu|\psi_I\rangle = \cos\,\alpha n^\mu(\theta_I,\phi_I) \tag{8}$$

for the local pseudospin density. Notice that for the case $\alpha \neq 0$ or π (i.e., $\cos^2\alpha < 1$), the local (pseudo)spin densities are no longer normalized, but are of length $|\mathbf{m}_{S/I}|^2=\cos^2\alpha$. Thus, in a semiclassical picture, the (pseudo)spin dynamics is no longer restricted to the surface of the Bloch sphere, but explores the entire volume enclosed by the sphere (Fig. 1).

B. Topological densities

For an SU(2) symmetry, spin textures in the 2D plane may be classified according to which homotopy class they belong. First, one needs to map the xy plane, by stereographic projection, onto the S^2 sphere. For an XYZ ferromagnet, the most general spin texture parametrization maps on the surface of the Bloch sphere S^2. The mappings $S^2 \to S^2$, which can be continuously deformed into one another, may be collected into homotopy classes.[36] The latter form a homotopy group $\pi_2(S^2)=\mathbb{Z}$. The elements of $\mathbb{Z}$, which are integers Q, characterize different topological sectors. Spin waves, for instance, belong to the topological sector with topological charge $Q=0$. Skyrmions carry a nonzero topological charge $Q\neq 0$. In the QH ferromagnet, a spin texture generates a charge density connected to the former through the so-called topological density. The topological density arises because an electron traveling in a spin texture acquires a Berry phase analogous to an Aharonov-Bohm phase. The total charge, expressed in units of the electron charge, of a spin texture in a QH state with Laughlin filling factor $\nu=1/(2m+1)$ is given by νQ.[16,17]

Next, we transpose these ideas to the larger SU(4) spin-pseudospin symmetry. With the help of the Schmidt decomposition, one may calculate the charge density induced by a general spin-pseudospin texture. When the internal states are described by a single SU(2) spin, the local density is simply given by the topological density of the associated director field, that is,

$$\rho_{\mathrm{top}} = \frac{\epsilon^{ij}}{8\pi}\mathbf{n}(\theta,\phi)\cdot[\partial_i\mathbf{n}(\theta,\phi)\times\partial_j\mathbf{n}(\theta,\phi)], \tag{9}$$

where ϵ^{ij} is the antisymmetric tensor, $\epsilon^{xy}=-\epsilon^{yx}=1$, and $\epsilon^{ii}=0$. To generalize this to the present case, it is sufficient to note that the spatial variation in $|\Psi(\mathbf{r})\rangle$ due to the texture

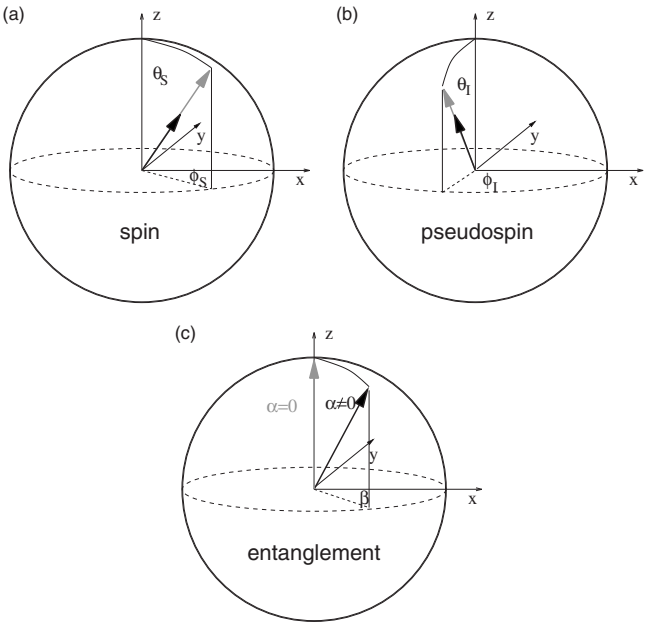

FIG. 1. Bloch spheres for entangled spin-pseudospin systems. Bloch sphere for (a) the spin, (b) pseudospin, and (c) a third type of spin representing the entanglement. In the case of spin-pseudospin entanglement ($|\cos\alpha| \neq 1$), the (pseudo)spin magnetizations explore the interior of their spheres, respectively (black arrows).

induces a Berry phase, which is encoded by the Berry connection,

$$\mathcal{A}(\mathbf{r}) = \frac{1}{i}\langle \Psi | \nabla \Psi \rangle. \tag{10}$$

The local charge density carried by the texture is then the 2D curl $\mathcal{B}(\mathbf{r}) = [\partial_x \mathcal{A}_y(\mathbf{r}) - \partial_y \mathcal{A}_x(\mathbf{r})]/(2\pi)$ of the fictitious vector potential $\mathcal{A}(\mathbf{r})$. After some simple algebra, we get

$$\mathcal{A}(\mathbf{r}) = \sin^2\frac{\alpha}{2}\nabla\beta + \cos\alpha\left(\sin^2\frac{\theta_S}{2}\nabla\phi_S + \sin^2\frac{\theta_I}{2}\nabla\phi_I\right), \tag{11}$$

the curl of which is, thus,

$$\mathcal{B}(\mathbf{r}) = \cos\alpha\{\rho_{\text{top}}[\mathbf{n}(\theta_S,\phi_S)] + \rho_{\text{top}}[\mathbf{n}(\theta_I,\phi_I)]\} + \rho_{\text{top}}[\mathbf{n}(\alpha,\beta)] + \sin^2\frac{\theta_S}{2}\rho_{\text{top}}[\mathbf{n}(\alpha,\phi_S)] + \sin^2\frac{\theta_I}{2}\rho_{\text{top}}[\mathbf{n}(\alpha,\phi_I)]. \tag{12}$$

III. SPIN-PSEUDOSPIN ENTANGLEMENT

A. Measure of entanglement

The above parametrization makes it clear that there are skyrmions in which spin and pseudospin can be perfectly entangled. This is most simply the case where for instance $|\psi_S\rangle = \binom{1}{0}$, $|\chi_S\rangle = \binom{0}{1}$, $|\psi_I\rangle = (1/\sqrt{2})\binom{1}{1}$, and $|\chi_I\rangle = (1/\sqrt{2})\binom{-1}{1}$ for all $\mathbf{r}$, and the skyrmion is a texture in $\alpha(\mathbf{r})$ and $\beta(\mathbf{r})$ only [which can take the same form as θ_S, ϕ_S in a pure spin skyrmion; this form is made explicit in Eq. (23) below]. In this case, it is easy to see, e.g., that $\sigma^x \equiv 0$ throughout as this operator is off-diagonal in this basis but has no matrix elements between $|\psi_S\rangle|\psi_I\rangle$ and $|\chi_S\rangle|\chi_I\rangle$. At the same time, σ^z has the same profile as in a standard spin skyrmion because its expectation value is simply given by $\cos\alpha(\mathbf{r})$.

The vanishing of the expectation value of the transverse components of the spin is, thus, a consequence of their being entangled with the pseudospin degree of freedom. To quantify this entanglement, we propose to use the following measure:

$$\Xi := 1 - \sum_a \langle \sigma^a \rangle^2 = 1 - \sum_\mu \langle \tau^\mu \rangle^2. \tag{13}$$

Equation (13) is easily expressed from the Schmidt decomposition [Eq. (2)] as

$$\Xi = \sin^2\alpha. \tag{14}$$

As a result, for the abovementioned entanglement texture, which may be visualized on a third Bloch sphere [Fig. 1(c)], local entanglement is minimal ($\Xi = 0$) when $\sin\alpha = 0$, that is, $\alpha = 0$ or $\alpha = \pi$, corresponding to the center of the texture or to the points at infinity. Entanglement is maximal ($\Xi = 1$) when $\alpha = \pi/2$, that is, at a distance from the origin given by the overall size λ of the texture. Note that at a maximally entangled point, the moduli of both spin and pseudospin vanish, as may be seen from Eqs. (7) and (8).

Alternatively, for the spinor defined in Eq. (6),

$$\Xi = 4|w_1 w_4 - w_2 w_3|^2. \tag{15}$$

For a factorizable state, in which the wave function can assume the form of an outer product between spin and pseudospin parts, $|\Psi_{\lambda\mu}\rangle = u_\lambda v_\mu$, one immediately finds $\Xi = 0$. Note that conversely, a vanishing Ξ implies that we have a factorizable state. For a completely entangled state, e.g., $w_1 = w_4 = 1/\sqrt{2}$, $w_2 = w_3 = 0$, we have $\Xi = 1$.

B. Degenerate texture families in the presence of spin anisotropy

In the presence of a Zeeman field, the SU(2) symmetry of the spin degree of freedom gets reduced to a U(1) symmetry of rotations around the z axis (along which we take the external field to be aligned). The generator of this symmetry is σ^z. We furthermore consider, for illustration reasons, that the SU(2) pseudospin symmetry is likewise broken to U(1), and we choose the z axis such that the rotations generated by τ^z, the z component of the pseudospin, commute with the underlying Hamiltonian. We discuss, in Sec. V, some physical examples, in the context of bilayer quantum Hall systems and graphene, where this situation arises.

Given that the underlying model Hamiltonian commutes with τ^z and with σ^z, it also commutes with their product, $\sigma^z\tau^z$. This means that a textured state $|\mathcal{T}\rangle$ belongs to a degenerate family of textures $|\mathcal{T}(\gamma)\rangle = \exp(i\gamma\tau^z\sigma^z)|\mathcal{T}\rangle$. The most interesting property of this latter symmetry operation is its ability to transform a factorizable state into an entangled one. Indeed, it acts on the four-component spinors according to $w_{1,4} \to w_{1,4}\exp(i\gamma)$ and $w_{2,3} \to w_{2,3}\exp(-i\gamma)$. In the process, $|w_1 w_4 - w_2 w_3|^2 \to |w_1 w_4|^2 + |w_2 w_3|^2 - [w_1 w_4 \bar{w}_2 \bar{w}_3 \exp(4i\gamma) + \text{c.c.}]$, where the bar indicates complex conjugation. Therefore, as γ varies, Ξ varies between $\Xi^{\min}_{\max}$ with

$$\Xi^{\min}_{\max} = 4(|w_1 w_4| \mp |w_2 w_3|)^2. \tag{16}$$

It is interesting to specify how one may, thus, create a maximally entangled state. This corresponds to $\Xi_{\max} = 1$, or equivalently to $|w_1| = |w_4|$ and $|w_2| = |w_3|$, because one may rewrite

$$\Xi_{\max} = 1 - [(|w_1| + |w_4|)^2 + (|w_2| + |w_3|)^2] \times [(|w_1| - |w_4|)^2 + (|w_2| - |w_3|)^2]. \tag{17}$$

Note that creation of a maximally entangled state starting from a factorized one is possible when the four spinor components have the same modulus. Another limiting case is obtained when $\Xi_{\min} = \Xi_{\max}$, that is, the action of the $\sigma^z\tau^z$ generator does not change the degree of entanglement, although the quantum state does change as the angle γ varies. This requires that at least one of the four spinor components vanishes. If the initial state is factorizable, this translates into $w_1 w_4 = w_2 w_3 = 0$.

IV. CONSEQUENCES OF ENTANGLEMENT

A. Descendants of skyrmions and bimerons

Let us now consider the effect of these entangling transformations on the textures that are most relevant for the

physics of the QH effect in a bilayer system at a total filling factor ν close to 1. We choose, as a starting point, a "bimeron" texture, $\mathcal{M}$, in which the spin is constant along the magnetic field and the pseudospin has a topologically nontrivial texture [see Eq. (28) below]. Due to the easy-plane anisotropy, the pseudospin is oriented in an arbitrary direction within the xy plane far from the meron core, whereas in the core region it is oriented in the $\pm z$ direction. There are furthermore two possible vorticities, such that one may distinguish between four meron types, each of which has half a charge.[16] A meron in itself costs a logarithmically large amount of energy due to the vorticity and must, therefore, be accompanied by a second meron of opposite vorticity in order to obtain a pseudospin texture of finite energy. If both merons have the same topological charge, one obtains a bimeron with an overall topological charge of ± 1, otherwise the bimeron is topologically connected to the (ferromagnetic) ground state. The action of τ^z on this state is simply to rotate the texture in the easy plane of the pseudospin, which is a global symmetry operation. The action of σ^z is trivial as all spins point in the z direction, and hence, a rotation about this axis has no effect. Therefore, the combined effect of $\tau^z\sigma^z$ is the same global rotation as that effected by τ^z alone, and no entanglement is generated. This is in agreement with the general discussion given above because we have for instance $w_3=w_4=0$ if all the spins are up, which clearly satisfies $w_1w_4=w_2w_3=0$.

Next, we consider Sondhi *et al.*'s original spin-skyrmion texture $|\mathcal{S}\rangle$, in which the pseudospin lies in a fixed direction in the xy plane (the x direction, say). The effect of a rotation generated by τ^z is simply to rotate the pseudospin uniformly about the z axis in pseudospin space. The effect of σ^z rotations is a global rotation of the spin texture about the z axis in spin space. Now, the crucial observation is that the effect of the combination $\tau^z\sigma^z$ is no longer just a trivial rotation. Rather, the operation generates a texture in which spin and pseudospin are entangled. To be more specific, we choose the pure spin texture as

$$|\mathcal{S}\rangle = \begin{pmatrix} \cos\frac{\theta(\mathbf{r})}{2} \\ \sin\frac{\theta(\mathbf{r})}{2} e^{i\phi(\mathbf{r})} \end{pmatrix}_S \otimes \frac{1}{\sqrt{2}}\begin{pmatrix} 1 \\ 1 \end{pmatrix}_I, \tag{18}$$

where $\mathbf{r}=(x,y)$ denotes the location in the plane to which the local spinor $|\mathcal{S}\rangle$ is associated. The second term in Eq. (18) precisely means that the pseudospin is homogeneously oriented in the x direction, whereas the first one describes the (pure) spin texture. For a usual skyrmion located at the origin, we have

$$\tan\frac{\theta(\mathbf{r})}{2} e^{i\phi(\mathbf{r})} = \frac{x+iy}{\lambda}, \tag{19}$$

where λ has the dimension of a length and corresponds to the spatial extension of the skyrmion. In this fully separable state, the expectation value of the spin operator reads

$$\langle\sigma^x\rangle = \frac{2\lambda x}{\lambda^2+x^2+y^2}, \tag{20}$$

$$\langle\sigma^y\rangle = \frac{2\lambda y}{\lambda^2+x^2+y^2}, \tag{21}$$

$$\langle\sigma^z\rangle = \frac{\lambda^2-x^2-y^2}{\lambda^2+x^2+y^2}, \tag{22}$$

which shows that the complex number $(x+iy)/\lambda$ is simply given by the stereographic projection from the south pole of the unit vector $\langle\boldsymbol{\sigma}\rangle$ onto the complex plane.

Let us now apply the symmetry unitary operation $\exp[i\frac{\pi}{4}(\sigma^z+1)(\tau^z-1)]$ to $|\mathcal{S}\rangle$. We, thus, obtain the state $|\mathcal{E}\rangle$, which may be written as

$$|\mathcal{E}\rangle = \cos\frac{\theta(\mathbf{r})}{2}\begin{pmatrix} 1 \\ 0 \end{pmatrix} \otimes \begin{pmatrix} 1 \\ -1 \end{pmatrix} + \sin\frac{\theta(\mathbf{r})}{2} e^{i\phi(\mathbf{r})}\begin{pmatrix} 0 \\ 1 \end{pmatrix} \otimes \begin{pmatrix} 1 \\ 1 \end{pmatrix}. \tag{23}$$

In this case, one recovers the pure entanglement texture mentioned at the beginning of Sec. III. As we have already mentioned there, $\langle\sigma^{x,y}\rangle=0$ in this state whereas the value of σ^z changes just as for an ordinary $\mathcal{S}$ spin texture. Likewise, we find that $\langle\tau^{y,z}\rangle=0$, and thus,

$$\langle\tau^x\rangle = -\cos\,\theta(\mathbf{r}) = -\frac{\lambda^2-\mathbf{r}^2}{\lambda^2+\mathbf{r}^2}. \tag{24}$$

B. General CP^3 skyrmions

Finally, it is interesting to extend this analysis to the most general CP^3 texture, subject to the condition that $\tau^x=-\sigma^z=1$ for the "point" $|z|=\infty$. It is generated by the local spinor $|\mathcal{G}\rangle$ defined by

$$|\mathcal{G}\rangle = (|\lambda_1|^2+|\lambda_2|^2+2|z|^2+2|b|^2)^{-1/2}\begin{pmatrix} \lambda_1 \\ \lambda_2 \\ z-b \\ z+b \end{pmatrix}, \tag{25}$$

where $z=x+iy$, and where we denote the normalization prefactor as $\mathcal{N}$ in what follows. Here λ_1, λ_2, and b are complex parameters. The quantity $|b|^2+(|\lambda_1|^2+|\lambda_2|^2)/2$ is the overall length scale of the texture. The physical meaning of these parameters is seen more explicitly, by considering special cases, which allow one to recover the two textures (18) and (23) already discussed,

$$|\mathcal{S}\rangle = (2\lambda_1^2+2|z|^2)^{-1/2}\begin{pmatrix} \lambda_1 \\ \lambda_1 \\ z \\ z \end{pmatrix}, \tag{26}$$

$$|\mathcal{E}\rangle = (2\lambda_1^2+2|z|^2)^{-1/2}\begin{pmatrix} \lambda_1 \\ -\lambda_1 \\ z \\ z \end{pmatrix}, \tag{27}$$

and the abovementioned bimeron texture

$$|\mathcal{M}\rangle = (2b^2 + 2|z|^2)^{-1/2} \begin{pmatrix} 0 \\ 0 \\ z-b \\ z+b \end{pmatrix}. \tag{28}$$

Further insight may be obtained by considering the effect of a uniform rotation by an angle γ of the spin around the z axis. This changes $(\lambda_1, \lambda_2, b)$ into $(e^{-i\gamma}\lambda_1, e^{-i\gamma}\lambda_2, b)$, after multiplying the spinor by a global phase that brings it back to the above form. Similarly, a uniform rotation along the x axis in pseudospin space can be represented by the matrix

$$\begin{pmatrix} e^{i\chi/2}\cos\frac{\chi}{2} & -ie^{i\chi/2}\sin\frac{\chi}{2} & 0 \\ -ie^{i\chi/2}\sin\frac{\chi}{2} & e^{i\chi/2}\cos\frac{\chi}{2} & 0 \\ 0 & 0 & e^{i\chi} \end{pmatrix} \tag{29}$$

acting on the column vector $(\lambda_1, \lambda_2, b)^T$.

What are the entanglement properties of $\mathcal{G}$? We define $2\lambda = \lambda_1 + \lambda_2$ and $2\delta = \lambda_1 - \lambda_2$ so that we obtain

$$\Xi = \frac{16}{\mathcal{N}^4}[|\delta^2 z^2| + |\lambda^2 b^2| + 2|\lambda\delta z b|\cos\phi], \tag{30}$$

where $\phi = \arg(z\bar{b}\bar{\lambda}\delta)$.

Hence, there are always two unentangled points, $\Xi = 0$, the one by construction at $|z| = \infty$ as well as one at $z_m = -b\lambda/\delta$, at which the spinor is given by

$$\frac{1}{\mathcal{N}} \begin{pmatrix} 1 \\ -\frac{2b}{\lambda_1 - \lambda_2} \end{pmatrix} \otimes \begin{pmatrix} \lambda_1 \\ \lambda_2 \end{pmatrix}.$$

To maximize the entanglement, let us first consider $|z|$ to be fixed. The above expression shows that we should pick $\phi = 0$, which means that z should belong to the line passing through z_m and the origin, in the direction opposite to z_m. It turns out that if z moves away from the origin along this half line, Ξ first increases, reaches a maximum for $|z| = |z_M|$, and then decreases. $|z_M|$ is given by

$$|z_M| = -\frac{|\lambda b|}{|\delta|} + \sqrt{(|b|^2 + |\delta|^2 + |\lambda|^2) + |b|^2|\lambda|^2/|\delta|^2}, \tag{31}$$

which moves to ∞ for $\delta = \lambda_1 - \lambda_2 = 0$.

From this expression, one can read off the following special cases. The *only* completely unentangled textures, $\Xi(z) \equiv 0$, are those with $\delta = 0$ and either $b = 0$ or $\lambda = 0$. The former corresponds to the skyrmion $\mathcal{S}$, the latter to the bimeron $\mathcal{M}$.

Complete entanglement at a point, $\Xi(z_M) = 1$, is achieved only in the case of $|\lambda| = |b|$ for any δ. The case $b = 0$ corresponds to the entanglement skyrmion $\mathcal{E}$ introduced above. The special feature of $b = 0$ is that maximal entanglement is obtained not just at two isolated points but on the circle $|z_M| = |\lambda_1|$. In that sense, $\mathcal{E}$ is the most entangled texture.

We may, furthermore, study the "entanglement operator"

$$\Gamma(\gamma) = \exp[i\gamma\tau^z(1 + \sigma^z)], \tag{32}$$

which transforms $\mathcal{G}$ into $\mathcal{G}'$ by replacing

$$\lambda_1' = \lambda_1 \exp[2i\gamma], \quad \lambda_2' = \lambda_2 \exp[-2i\gamma]. \tag{33}$$

Otherwise, the structure of the relevant equations remains unchanged, and λ and δ become

$$\lambda' = \lambda\cos(2\gamma) + i\delta\sin(2\gamma),$$

$$\delta' = \delta\cos(2\gamma) + i\lambda\sin(2\gamma).$$

These equations show that λ' moves along an elliptical orbit in the complex plane. In the case where the modulus of b lies between those of the major and minor axes of the ellipse (λ and δ if they are real), there will thus be a value of γ for which maximal entanglement occurs.

V. ENERGY SCALES AND ANISOTROPIES IN BILAYERS QH SYSTEMS AND GRAPHENE

A. Bilayer Hamiltonian

In terms of the density operators defined in the Appendix, the Hamiltonian for a bilayer quantum Hall system, taking into account both spin and pseudospin degrees of freedom, reads

$$H = \frac{1}{2}\sum_{\mathbf{q}} V_+(\mathbf{q})\bar{\rho}(-\mathbf{q})\bar{\rho}(\mathbf{q}) + 2\sum_{\mathbf{q}} V_-(\mathbf{q})\bar{P}^z(-\mathbf{q})\bar{P}^z(\mathbf{q}) + \Delta_Z\bar{S}^z(\mathbf{q}=0) + \Delta_T\bar{P}^x(\mathbf{q}=0) + \Delta_I\bar{P}^z(\mathbf{q}=0), \tag{34}$$

where the first two terms are due to the different intralayer and interlayer electron-electron interactions, with

$$V_\pm(\mathbf{q}) = \frac{\pi e^2}{\epsilon q}e^{-q^2/2}(1 \pm e^{-qd}),$$

in terms of the layer separation d and the dielectric constant ϵ. The last three terms in Eq. (34) are Zeeman-type terms; the first one is indeed the Zeeman term that acts on the z component of the spin density, whereas the second one is due to interlayer tunneling, and the last one is a layer imbalance term which may be tuned by applying a gate voltage. Whereas the Zeeman-type terms break the SU(4) symmetry explicitly, the first interaction term is SU(4) symmetric, and the second one gives rise to an easy-plane anisotropy for the pseudospin magnetization, and thus breaks the SU(2) pseudospin symmetry down to U(1).

In the case of GaAs heterostructures, we have the energy scales (for a dielectric constant of $\epsilon \sim 13$ and an effective spin coupling $g = -0.44$) in Table I where the last term is sample dependent. It can, for instance, be varied by considering samples with different distance between the layers. Indeed, the tunneling term Δ_T can vary over a rather large range and—most importantly—it may become the smallest of these energy scales. One notices that the largest energy scale is given by the interaction energy. Strictly speaking, the characteristic intralayer interaction is given by $e^2/\epsilon l_B$, whereas the interlayer correlations are governed by

TABLE I. Energy scales for a bilayer QH system in GaAs heterostructures.

Energy	Value for arbitrary B	Value for $B=6$ T ($\nu=1$)
$e^2/\epsilon l_B$	$50\sqrt{B[T]}$ K	122 K
Δ_Z	$0.33B$[T] K	2 K
Δ_T		$0,\ldots,100$ K

$e^2/\epsilon\sqrt{d^2+l_B^2}$. However, we typically have $d\sim l_B=26/\sqrt{B[\mathrm{T}]}$ nm. The Zeeman term is roughly two orders of magnitude smaller than the characteristic interaction energy. This means that although both the Zeeman effect and interlayer tunneling tend to fully polarize the system, with the spin aligned along the z axis and the pseudospin along the x axis, this polarization only occurs subsequent to the onset of ferromagnetic order.

Notice that the Hamiltonian [Eq. (34)] also applies to the case of graphene, a system which is, however, less anisotropic than bilayer GaAs heterostructures. The interactions are dominated by the symmetric part, $V_+(\mathbf{q})$, of the interaction, whereas symmetry-breaking interactions are suppressed by a factor a/l_B, in terms of the carbon-carbon distance $a=0.14$ nm,[11,12,37] which replaces d as the second characteristic length scale. As for GaAs heterostructures, the Zeeman effect in graphene plays a minor role as compared to the leading interaction energy scale. Concerning possible Zeeman-type terms acting on the pseudospin, which describes the two inequivalent Dirac points, their existence remains an open and intense field of research.[38–40] However, these terms are expected to be also small with respect to the interaction energy. The energy scales for graphene are summarized in Table II (for typical values $\epsilon\sim 2.5$ and $g\sim 2$). We have displayed the values both for 6T and for 25T because the filling factor $\nu=1$ may be obtained for different values of the magnetic field due to a control of the carrier density by application of a gate voltage. The latter choice (25T) is motivated by the fact that above this value, the $\nu=1$ QH plateau, is well developed.[41]

B. Physical relevance of entanglement in bilayer systems and graphene

The above considerations and the possibility of entangled texture states sensitively depend on the smallness of the tunneling gap in bilayer systems. Experimentally, a small tunneling gap is a reasonable assumption as discussed above, and we consider the case $\Delta_T=0$ in the following.

TABLE II. Energy scales in graphene.

Energy	Value for arbitrary B	Value for $B=6$ T	Value for $B=25$ T
$e^2/\epsilon l_B$	$250\sqrt{B[\mathrm{T}]}$ K	620 K	1250 K
Δ_Z	$1.2B$[T] K	7 K	30 K
$\Delta_{sb}<(e^2/\epsilon l_B)(a/l_B)$	$<1B$[T] K	<6 K	<25 K

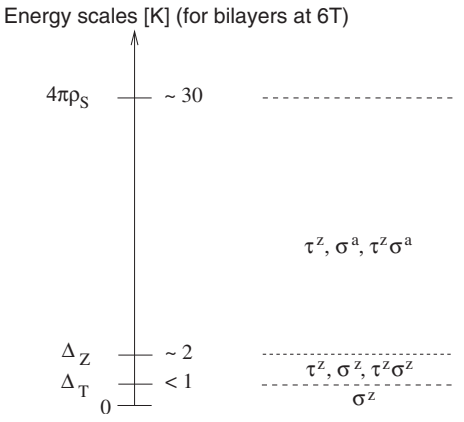

FIG. 2. Energy scales for GaAs bilayer QH system for a magnetic field of $B=6$ T. The spin stiffness is given by $\rho_S=(16\sqrt{2\pi})^{-1}e^2/(l_B\epsilon)$. On the right-hand side (RHS), we indicate the symmetry generators for the Hamiltonian obtained by neglecting terms with energy scales below k_BT.

In the temperature regime $T<\Delta_Z$, one may then find entangled states with an internal symmetry spanned by the Cartan algebra $\{\tau^z,\sigma^z,\tau^z\sigma^z\}$ of the SU(4) group (Fig. 2). As shown above, the degeneracy supports entangled texture states in this regime. In the absence of Δ_Z, further entangled states arise, described by an $\mathrm{SU}(2)\times\mathrm{U}(1)$ symmetry group, which is larger and non-Abelian—the operators $\{\tau^z,\sigma^a,\tau^z\sigma^a\}$ do not all commute due to the algebra satisfied by the Pauli matrices σ^a (see Appendix A). This means that one may choose any σ^a, instead of just σ^z, to create entangled states, with the help of the entanglement operator

$$\Gamma(\gamma^a)=\exp[i\gamma^a\tau^z(1+\sigma^a)],$$

which generalizes that in Eq. (32). A full analysis of skyrmions in this regime is deferred to future work.

The graphene case is quite similar. The energy scales are shown in Fig. 3, for a characteristic field of $B=25$ T, where the $\nu=1$ plateau in the Hall resistance is well established.[41] The interaction potential has been shown to be SU(4) symmetric over a large temperature range, and a broken

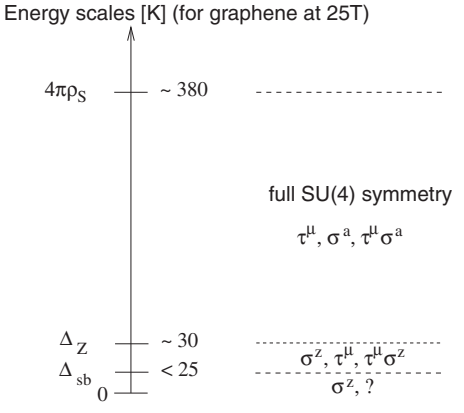

FIG. 3. Energy scales for graphene in $B=25$ T. On the RHS, we indicate the symmetry generators for the Hamiltonian obtained by neglecting terms with energy scales below k_BT.

SU(2) pseudospin symmetry due to lattice effects is expected only below an energy scale $\Delta_{sb} \sim (e^2/\epsilon l_B)(a/l_B) \sim B[\mathrm{T}]$ K.[11,12,37,39] The nature of this symmetry breaking differs in the relativistic LLs $|n| \geq 1$ from that in the central one $n=0$. For $|n| \geq 1$, one expects an easy-plane anisotropy,[11] which supports entangled states with an internal symmetry generated by $\{\tau^z, \sigma^z, \tau^z\sigma^z\}$, similar to the bilayer case in the regime $\Delta_T < T < \Delta_Z$. The $n=0$ case is more involved, and the easy-plane anisotropy of the pseudospin magnetization[11,37] is in competition with an easy-axis anisotropy,[12,39] which may lead to a residual Z_2 pseudospin symmetry. However, in all cases numerical prefactors strongly suppress the energy scale for lattice effects $\Delta_{sb} \sim (e^2/\epsilon l_B)(a/l_B)$ below the typical Zeeman energy scale $\Delta_Z \sim 1.2B[\mathrm{T}]$ K.

In an intermediate regime of $\Delta_{sb} < T < \Delta_Z$, the internal symmetry is given by $\{\tau^\mu, \sigma^z, \tau^\mu\sigma^z\}$, which supports entangled texture states. For temperatures well above Δ_Z, one recovers in turn the full SU(4) symmetries, and SU(4) skyrmions[21–23] are expected to be the relevant charged excitations.

VI. DYNAMICAL PROPERTIES OF ENTANGLED TEXTURES

One strong experimental motivation for the present work has been the experimental observation of nuclear spin relaxation[32,33] in the vicinity of the transition between the quantum Hall pseudospin ferromagnetic phase and the compressible phase in a bilayer system at total filling factor $\nu=1$, where the control parameter is the ratio d/l_B. These two studies agree on the fact that nuclear relaxation is much faster in the compressible phase than in the quantum Hall phase. What is particularly striking is that a slight deviation of the total filling factor away from $\nu=1$ in the quantum Hall phase induces a significant increase in the relaxation rate $1/T_1$. Such a strong variation with the filling factor is reminiscent of what has been observed in a monolayer at $\nu=1$,[15] where the additional relaxation is attributed to the gapless spin modes induced by the presence of skyrmions.[25] In the context of a bilayer, this was surprising because the samples are widely believed to be fully spin polarized in their quantum Hall phase at $\nu=1$, and therefore, the charged textures would be pseudospin bimerons, which do not couple to nuclear spins. The dominant interpretation of these data is based on the idea of a coexistence between both quantum Hall and compressible phases in the vicinity of the transition.[32,33] This idea has been first proposed[42] to explain the strong longitudinal Coulomb drag peak observed in the vicinity of the transition[43] and is supported, on the theoretical side, by numerical diagonalization studies[44] which point toward a first-order transition. Furthermore, some recent experiments have confirmed the fact that there exists a large jump in the spin polarization between the two phases.[45]

Here we would like to revive the case for another scenario. It is not clear to us why the compressible phases found either at $\nu=1$ and large d/l_B or away from $\nu=1$ for smaller d/l_B should have the same spin excitations. This assumption is supported by experimental results[32,33] which show a comparable $1/T_1$ in both cases [see for instance Figs. 3(b) and 3(c) in Ref. 32]. But theoretically, we may question why composite-fermion physics,[46] which is expected to emerge at large d/l_B with each layer at half filling, should remain relevant at small d/l_B and away from $\nu=1/2$ per layer. Note however that numerical[47,48] and analytical[49] calculations indicate that even for a homogeneous system, a small but nonzero layer separation admixes composite-fermion components to the incompressible superfluid state. An alternative way to account for the strong relaxation away from $\nu=1$ in the gapped phase is to assume the presence of entangled textures. On purely energetic grounds, the pure spin texture is not favorable because of the large Zeeman energy. We may then expect that an entangled texture would have a significantly lower energy than a spin texture, and that it can still contribute to nuclear spin relaxation. It has in fact been shown that a lattice of entangled skyrmions has even a lower energy than a lattice of spin-polarized bimerons if d/l_B is large enough and the Zeeman coupling is not too large.[29] Leaving aside these delicate energetic questions, which require to optimize the CP^3 profile in the presence of the various anisotropies,[28,29] we now briefly address the question of the collective excitations around an entangled texture, and their impact on electronic spin-spin correlation functions. Note that detailed numerical calculations of the collective modes for CP^3 skyrmion crystals are available.[30] Here, we would like simply to present a simple framework to analyze the small fluctuations around an entangled texture, focusing on the counting of zero modes. A striking result is that the NMR relaxation rate induced by spin fluctuations around a given texture is changed when this texture is modified by the application of the entanglement operator $\exp(i\gamma\sigma^z\tau^z)$, even when this operator is an exact symmetry of the Hamiltonian, i.e., when Δ_T [see Eq. (34)] vanishes.

For simplicity, we consider the SU(4) symmetric case. In this situation, the general texture that carries a unit topological charge has the form[50]

$$\vec{w}(z) = z\vec{u} + \vec{v}, \tag{35}$$

where $\vec{w}(z)$ parametrizes in fact the ray in CP^3 that contains this vector. Because both $\vec{u}=(u_1,u_2,u_3,u_4)$ and $\vec{v}=(v_1,v_2,v_3,v_4)$ have four complex components, we have a seven complex parameter family of degenerate textures, after factoring out the simultaneous multiplication of $\vec{u}$ and $\vec{v}$ by the same arbitrary complex number. We, therefore, expect seven zero modes for the dynamics of small fluctuations around such texture. Note that in the absence of the texture, $\vec{w}(z)$ is constant so there are three zero modes that may be attributed to the ferromagnetic vacuum sector and four to the texture: one of them corresponds to a translation $(z \to z+a)$ and the three remaining ones to the three independent directions in the internal space of CP^3.

It is in fact illuminating to consider the case of q textures. Then, the minimal energy configurations are described as[50]

$$\vec{w}(z) = \sum_{j=0}^{q} z^j \vec{u}_j, \tag{36}$$

where the N-component $q+1$ complex vectors $\vec{u}_j$ are arbitrary. We have, therefore, a highly deformable system where

$(q+1)N-1$ degrees of freedom exhibit no restoring force. For clarity, we are generalizing here to the CP^{N-1} model with global SU(N) symmetry, N being equal to four in the case of a bilayer. Removing the $N-1$ degrees of freedom associated with the ferromagnetic vacuum sector leaves qN of them attached to the q textures, so finally, there are N static degrees of freedom per texture. Note that the SU(N) symmetric CP^{N-1} model describes a very special system, where the textures do not interact. In reality, various anisotropies and also the long-range Coulomb interaction between the electric charges bound to the textures lift this massive degeneracy within this ideal q-skyrmion manifold, stabilizing most likely a crystal of skyrmions. Without anisotropies, nor Coulomb repulsion, the qN static degrees of freedom describing the small deformations around such crystal can be organized into N nondispersive Bloch bands. In the presence of realistic anisotropies and the Coulomb repulsion, these bands acquire a dispersive character. Clearly, one of these N branches of the collective spectrum will be a magnetic-field phonon mode, with[51] $\omega \simeq |q|^{3/2}$, and $N-1$ other branches will be Goldstone-type modes. We, therefore, recover the counting that emerged from a more microscopic analysis.[23]

Let us now return to the quantum dynamics of the electron system around a single texture. As in Refs. 24–26 and 30, we consider the framework of the time-dependent Hartree-Fock (TDHF) approximation, which can be formulated in several different ways. A rather appealing one consists of viewing the set of Slater determinants as a classical phase space.[52] The Hartree-Fock Hamiltonian is then used as a classical Hamiltonian that generates the same dynamics as the TDHF equations of motion. In our problem of a filled LL, we also assume (see the beginning of Sec. II) that the occupied single-particle states correspond to localized four-component spinors $w_j(\mathbf{r})$ that are *not* normalized here. Indeed, dropping the normalization constraint simplifies the equation of motion at the expense of introducing a form of a generalized local gauge symmetry $w_j(\mathbf{r}) \to h(\mathbf{r}) w_j(\mathbf{r})$, which has to be factored out in the overall mode counting. The Hartree-Fock Hamiltonian may be taken [assuming SU(4) symmetry] as

$$H(\{w\}) = \frac{1}{4}\int d^2r \left(\frac{(\nabla w, \nabla w)}{(w,w)} - \frac{(\nabla w, w)(w, \nabla w)}{(w,w)^2} \right), \quad (37)$$

where the inner product is defined by $(w,w') = \Sigma_{j=1}^{4} \bar{w}_j(\mathbf{r}) w'_j(\mathbf{r})$. This is the only local Hamiltonian that is quadratic in gradients and invariant under the global SU(4) transformations in spinor space and also under local gauge transformations $w_j(\mathbf{r}) \to h(\mathbf{r}) w_j(\mathbf{r})$.[50] As usual, it is now convenient to introduce the complex position coordinate $z = x + iy$ such that

$$H(\{w\}) = \frac{1}{2}\int d^2r \left(\frac{(\bar{\partial} w, \partial w) + (\partial w, \bar{\partial} w)}{(w,w)} \right) - \frac{(\bar{\partial} w, w)(w, \partial w) + (\partial w, w)(w, \bar{\partial} w)}{(w,w)^2}.$$

The notations mean in particular that $(\partial w, w') = \Sigma_j (\partial_z \bar{w}_j) w'_j$ and $(\bar{\partial} w, w') = \Sigma_j (\partial_{\bar{z}} \bar{w}_j) w'_j$. The classical Hamiltonian equations of motions are

$$i\frac{\partial}{\partial t} w_j(\mathbf{r},t) = \frac{\delta H}{\delta w_j(\mathbf{r})},$$

$$i\frac{\partial}{\partial t} \bar{w}_j(\mathbf{r},t) = -\frac{\delta H}{\delta \bar{w}_j(\mathbf{r})}. \quad (38)$$

Because of the local gauge invariance, the norm $(w(\mathbf{r}), w(\mathbf{r}))$ is conserved for any $\mathbf{r}$. The price to pay for this is that the equations of motion are rather complicated. Using the gauge symmetry, we may modify Eq. (38) by a term proportional to $w_j(\mathbf{r})$ that simplifies it considerably, giving up the conservation of $(w(\mathbf{r}), w(\mathbf{r}))$, while preserving the ray of $w(\mathbf{r})$ in CP^3 and, therefore, the physical content of the solutions. This simplified equation of motion reads

$$i\frac{\partial}{\partial t} w = -\partial^2_{z,\bar{z}} w + \frac{(w, \partial_{\bar{z}} w)}{(w,w)} \partial_z w + \frac{(w, \partial_z w)}{(w,w)} \partial_{\bar{z}} w + \lambda(\mathbf{r},t) w, \quad (39)$$

where $\lambda(\mathbf{r},t)$ is an arbitrary complex function of $\mathbf{r}$ and t, and $\partial^2_{z,\bar{z}} \equiv \partial_z \partial_{\bar{z}}$. Note that the gauge transformation $w'(\mathbf{r},t) = h(\mathbf{r},t) w(\mathbf{r},t)$ sends a solution w into another solution w' provided λ is changed into λ' given by

$$\lambda' = \lambda + h^{-1}\left[i\frac{\partial h}{\partial t} + \partial^2_{z,\bar{z}} h - \frac{(w, \partial_{\bar{z}} w)}{(w,w)} \partial_z h - \frac{(w, \partial_z w)}{(w,w)} \partial_{\bar{z}} h \right] - 2\frac{\partial_{\bar{z}} h \partial_z h}{h^2}.$$

It is immediate to check that the general static texture $w(\mathbf{r}) = zu + v$ is indeed a solution with $\lambda = 0$.

Linearizing the equations of motion around these static solutions gives

$$i\frac{\partial}{\partial t} \epsilon = -\partial^2_{z,\bar{z}} \epsilon + \frac{(w, \partial_{\bar{z}} w)}{(w,w)} \partial_z \epsilon + \frac{(w, \partial_z w)}{(w,w)} \partial_{\bar{z}} \epsilon + \lambda(\mathbf{r},t) w, \quad (40)$$

where $\epsilon(\mathbf{r},t)$ denotes an infinitesimal variation and we have used the fact that $\partial_{\bar{z}} w = 0$ for the static texture. Note that λ is an infinitesimal complex function of the same order as ϵ. A first-order infinitesimal gauge transformation with $h(\mathbf{r},t) = 1 + \zeta(\mathbf{r},t)$ acts as

$$\epsilon' = \epsilon + \zeta w,$$

$$\lambda' = \lambda + i\frac{\partial \zeta}{\partial t} + \partial^2_{z,\bar{z}} \zeta - \frac{(w, \partial_z w)}{(w,w)} \partial_{\bar{z}} \zeta.$$

The eigenmodes have the form $\epsilon(\mathbf{r},t) = \epsilon(\mathbf{r}) e^{-i\omega t}$. Because the classical Hamiltonian is bounded below, ω can take only non-negative values. The zero modes are obtained from the condition $\partial_{\bar{z}} \epsilon = 0$, and the constraint of a fixed topological charge imposes that ϵ should be a polynomial of degree 1 in z. This yields an eight-dimensional space of zero modes in which the pure gauge transformations $\epsilon = \zeta_0 w$ with ζ_0 con-

stant in space and time, have to be removed. We, therefore, recover the seven-dimensional complex space of zero modes discussed at the beginning of this section.

Note that we have a conserved Hermitian form $\Omega(\eta,\xi)$ for any pair η,ξ of solutions of the linearized equations of motion [Eq. (40)]. This form Ω is defined by

$$\Omega(\eta,\xi)=\int d\mathbf{r}\frac{(\eta_\perp,\xi_\perp)}{(w,w)}=\int d\mathbf{r}\left(\frac{(\eta,\xi)}{(w,w)}-\frac{(\eta,w)(w,\xi)}{(w,w)^2}\right) \tag{41}$$

and is invariant under any local gauge transformation that affects simultaneously w, η, and ξ. In particular, for eigenmodes $\eta(\mathbf{r},t)=\eta(\mathbf{r})e^{-i\omega_\eta t}$ and $\xi(\mathbf{r},t)=\xi(\mathbf{r})e^{-i\omega_\xi t}$, we have $\Omega(\eta,\xi)=0$ as soon as $\omega_\eta\neq\omega_\xi$. This shows that a complete eigenmode basis $\epsilon^{\alpha,\omega}(\mathbf{r})$ (α being an internal polarization label) can be chosen to be orthogonal for the Hermitian form Ω.

We will not try to find the full continuous spectrum of the scattering problem defined by Eq. (40). Instead, we shall now consider the effect of the entanglement operator $\exp(i\gamma\sigma^z\tau^z)$ on the local spin-correlation function $C(\mathbf{r},\omega)=\int dt\langle S^+(\mathbf{r},t)S^-(\mathbf{r},t=0)\rangle e^{i\omega t}$ that controls the local nuclear spin-relaxation rate at the position $\mathbf{r}$. Here, $S^\pm(\mathbf{r},t)=S^x(\mathbf{r},t)\pm iS^y(\mathbf{r},t)$, in terms of the local spin densities $S^{x/y}(\mathbf{r},t)$. In the presence of a texture, translation invariance is lost so this correlation function will explicitly depend on $\mathbf{r}$. The TDHF approximation does not give us directly wave functions for collective modes so we use it to express the corresponding response function $R(\mathbf{r},\omega)=\frac{i}{\hbar}\int dt\langle[S_{\mathbf{r}}^+(t),S_{\mathbf{r}}^-(0)]\rangle e^{i\omega t}$ in terms of a complete basis of eigenmodes $\epsilon^{\alpha,\omega}$. $R(\mathbf{r},\omega)$ is related to the correlation function by the usual fluctuation-dissipation formula,

$$C(\mathbf{r},\omega)=\frac{2\hbar}{1-e^{-\beta\hbar\omega}}\Im R(\mathbf{r},\omega). \tag{42}$$

Introducing the 4×4 matrices $M^\pm=\sigma^\pm_{\text{spin}}\otimes\mathbb{1}_{\text{iso}}$, the response function is then expressed as

$$\begin{aligned}\Im R(\mathbf{r},\omega)=&\pi\sum_\alpha\frac{[w(\mathbf{r}),M^+\epsilon_\perp^{\alpha,\omega}(\mathbf{r})][\epsilon_\perp^{\alpha,\omega}(\mathbf{r}),M^-w(\mathbf{r})]}{[w(\mathbf{r}),w(\mathbf{r})]^2}\theta(\omega)\\&-\pi\sum_\alpha\frac{[w(\mathbf{r}),M^-\epsilon_\perp^{\alpha,-\omega}(\mathbf{r})][\epsilon_\perp^{\alpha,-\omega}(\mathbf{r}),M^+w(\mathbf{r})]}{[w(\mathbf{r}),w(\mathbf{r})]^2}\\&\times\theta(-\omega).\end{aligned} \tag{43}$$

Notice that we have treated, within the calculation of the low-energy modes, the skyrmion as a classical object, which is a valid approximation for large skyrmions, $\lambda\gg l_B$. For smaller skyrmions, the translational modes may still be treated on the classical level, whereas the rotational modes need to be quantized.[17]

Now, let us start from the pure spin texture discussed in Sec. IV and let us apply the entanglement operator $\exp(i\gamma\sigma^z\tau^z)$ to it. This unitary transformation in the full quantum Hilbert space induces a canonical transformation on the classical phase space of Slater determinants. It is, therefore, equivalent to compute the correlation function $\langle S^+S^-\rangle$ around the transformed texture and the correlation function $\langle S^+(\gamma)S^-(\gamma)\rangle$ around the original one, where $\mathbf{S}(\gamma)=\exp\times(-i\gamma\sigma^z\tau^z)\mathbf{S}\exp(i\gamma\sigma^z\tau^z)$. Explicitly, we obtain

$$S^\pm(\gamma)=\cos(2\gamma)S^\pm\otimes\mathbb{1}\mp i\sin(2\gamma)S^\pm\otimes\tau^z. \tag{44}$$

For the fluctuations around the pure spin texture, a little inspection shows that the τ^x component of the pseudospin is conserved. Therefore, crossed terms involving only one τ^z operator do not contribute to the sum over eigenmodes [Eq. (43)]. We finally get

$$\langle S^+S^-\rangle_\gamma=\cos^2(2\gamma)\langle S^+S^-\rangle_{\gamma=0}+\sin^2(2\gamma)\langle(S^+\tau^z)(S^-\tau^z)\rangle_{\gamma=0}. \tag{45}$$

Note that the two correlation functions that appear on the RHS of the above equation will in general differ because we are considering *local* spin and pseudospin operators. So the two τ^z operators taken at two different times are not expected to commute, in spite of the fact that the z component of the *total* pseudospin is conserved. This expression is quite interesting because it exhibits a competition between two effects. When γ increases slightly away from zero, the first term decreases, in agreement with physical intuition—the local spin is reduced by entanglement, and so is its contribution to NMR relaxation. Such scenario would be consistent with the experimental observation that $1/T_1$ increases faster for a monolayer than for a bilayer as the filling factor is moved away from the $\nu=1$ value (see for instance Fig. 4 of Ref. 33). But this is not the only effect induced by entanglement—the second term also builds up, showing that new relaxation channels occur, which correspond to flipping simultaneously both spin and pseudospin degrees of freedom.

A physical consequence of this variation in $1/T_1$ with the entanglement parameter γ could be the existence of large fluctuations in the nuclear relaxation rate from one sample to another, or for the same sample after thermal cycling between the low-temperature quantum Hall state and the normal electron fluid. Indeed, we may speculate that in the vicinity of the bilayer phase transition, the energy landscape in the space of possible textures is characterized by a rather flat minimum around the bimeron texture, and that it may then be difficult for the system to relax to its absolute ground state. If this picture were to be confirmed, the above discussion shows that $1/T_1$ would depend on the actual degree of entanglement reached by the system.

VII. SUMMARY AND OUTLOOK

In view of the intense current interest in the physics of entanglement—in part motivated by the experimental advances in cold atoms, the search for exotic electronic phases, and attempts to build a quantum computer—quantum Hall systems present an attractive subject of study, not least given the presence of several phases exhibiting macroscopic quantum coherence.

We have investigated the possible entanglement between two internal SU(2) degrees of freedom of electrons restricted to a single LL. Whereas the physical spin constitutes one SU(2) copy, the second one describes a pseudospin degree of freedom such as the layer index in bilayer QH systems or the

valley degeneracy in graphene in a strong magnetic field. The Schmidt decomposition allows one to treat both on an equal footing, while embedding them in a larger SU(4) space. This has enabled us to study the effects of realistic anisotropies in a transparent manner. In particular, by defining an entanglement operator which generates entire families of degenerate skyrmions, we are able to construct wave functions for entanglement skyrmions which are easy to visualize.

It has also become apparent that the NMR response of such multicomponent systems is affected by the degree of entanglement. Indeed, it remains to be seen whether this may provide an alternative to the puddle model of coexistence of a spin-polarized incompressible and a partially polarized compressible metallic phase,[42] which is mainly invoked in the explanation of the increased NMR relaxation rate when driving the total filling factor away from $\nu_T=1$.[32,33] Unfortunately, in graphene, where anisotropies in the valley sector are quite weak, NMR measurements turn out to be difficult because the majority ($\sim$99%) of the carbon atoms are ^{12}C isotopes, which are NMR inactive due to a zero nuclear spin.

This work leaves many open questions. The first is to identify precisely the regimes in which entangled textures can be stabilized as the absolute energy minima for charged excitations. This has been demonstrated to occur in the presence of charge imbalance between the two layers,[28] or even for the balanced system, for a layer separation lower than, but close to the critical one, provided the Zeeman energy is not too large.[29] An important issue here would be to understand the effect of random impurities that may disorder such lattices of entangled skyrmions and, thus, modify the energy balance between various configurations. But even when the spin-polarized bimeron is the most favorable texture, it would be very interesting to understand better the energy landscape in its vicinity because available numerical results suggest it may be rather flat,[29] which raises the possibility of a slow dynamics and a lack of equilibration. Finally, there exist certainly many other physical signatures of spin-pseudospin entanglement besides the local reduction in the magnitude of the average spin and pseudospin vectors. These issues are left for future studies.

ACKNOWLEDGMENTS

B.D. and M.O.G. thank the Rudolf Peierls Centre for Theoretical Physics, Oxford University, where much of this work was undertaken, for hospitality. P.L. acknowledges hospitality of the Departamento de Fisica (UFPE, Recife, Brazil) and the PVE/CAPES program. M.O.G. and P.L. acknowledge financial support by the Agence Nationale de la Recherche under Grant No. ANR-06-NANO-019-03.

APPENDIX: LOWEST-LL ALGEBRA FOR MULTICOMPONENT SYSTEMS

The local spin and pseudospin densities may be expressed in terms of Pauli matrices as

$$\bar{S}^a(\mathbf{r}) = \frac{1}{2} f(\mathbf{r}) \otimes (\sigma^a \otimes \mathbb{1}) \tag{A1}$$

and

$$\bar{P}^\mu(\mathbf{r}) = \frac{1}{2} f(\mathbf{r}) \otimes (\mathbb{1} \otimes \tau^\mu). \tag{A2}$$

Similarly, the total (charge) density may be written as

$$\bar{\rho}(\mathbf{r}) = f(\mathbf{r}) \otimes (\mathbb{1} \otimes \mathbb{1}). \tag{A3}$$

Here, $f(\mathbf{r})$ is the U(1) one-particle density projected to the lowest LL, the Fourier components of which satisfy the magnetic-translation algebra[16,53]

$$[f(\mathbf{q}), f(\mathbf{q}')] = 2i \sin\left(\frac{\mathbf{q} \wedge \mathbf{q}'}{2}\right) f(\mathbf{q}+\mathbf{q}') \tag{A4}$$

and

$$\{f(\mathbf{q}), f(\mathbf{q}')\} = 2 \cos\left(\frac{\mathbf{q} \wedge \mathbf{q}'}{2}\right) f(\mathbf{q}+\mathbf{q}'). \tag{A5}$$

In Eqs. (A1)–(A3), the bar indicates that the density operators are restricted to the lowest LL. Because of Eqs. (A4) and (A5), the Fourier-transformed density operators satisfy the commutation relations

$$[\bar{\rho}(\mathbf{q}), \bar{\rho}(\mathbf{q}')] = 2i \sin\left(\frac{\mathbf{q} \wedge \mathbf{q}'}{2}\right) \bar{\rho}(\mathbf{q}+\mathbf{q}'), \tag{A6}$$

$$[\bar{S}^a(\mathbf{q}), \bar{\rho}(\mathbf{q}')] = 2i \sin\left(\frac{\mathbf{q} \wedge \mathbf{q}'}{2}\right) \bar{S}^a(\mathbf{q}+\mathbf{q}'), \tag{A7}$$

$$[\bar{P}^\mu(\mathbf{q}), \bar{\rho}(\mathbf{q}')] = 2i \sin\left(\frac{\mathbf{q} \wedge \mathbf{q}'}{2}\right) \bar{P}^\mu(\mathbf{q}+\mathbf{q}'), \tag{A8}$$

$$[\bar{S}^a(\mathbf{q}), \bar{S}^b(\mathbf{q}')] = \frac{i}{2} \delta^{ab} \sin\left(\frac{\mathbf{q} \wedge \mathbf{q}'}{2}\right) \bar{\rho}(\mathbf{q}+\mathbf{q}') + i\epsilon^{abc} \cos\left(\frac{\mathbf{q} \wedge \mathbf{q}'}{2}\right) \bar{S}^c(\mathbf{q}+\mathbf{q}'), \tag{A9}$$

and

$$[\bar{P}^\mu(\mathbf{q}), \bar{P}^\nu(\mathbf{q}')] = \frac{i}{2} \delta^{\mu\nu} \sin\left(\frac{\mathbf{q} \wedge \mathbf{q}'}{2}\right) \bar{\rho}(\mathbf{q}+\mathbf{q}') + i\epsilon^{\mu\nu\sigma} \cos\left(\frac{\mathbf{q} \wedge \mathbf{q}'}{2}\right) \bar{P}^\sigma(\mathbf{q}+\mathbf{q}'). \tag{A10}$$

These commutation relations are directly obtained from the relation

$$[f(\mathbf{q}) \otimes A, f(\mathbf{q}') \otimes B] = \frac{1}{2}[f(\mathbf{q}), f(\mathbf{q}')] \otimes \{A,B\} + \{f(\mathbf{q}), f(\mathbf{q}')\} \otimes [A,B] \tag{A11}$$

for any pair of operators A, B. Furthermore, one obtains the mixed spin-pseudospin commutator,

$$[\bar{S}^a(\mathbf{q}),\bar{P}^\mu(\mathbf{q}')] = \frac{i}{2}\sin\left(\frac{\mathbf{q}\wedge\mathbf{q}'}{2}\right) f(\mathbf{q}+\mathbf{q}')\otimes(\sigma^a\otimes\tau^\mu). \tag{A12}$$

Naively, one might have expected that the spin and pseudospin densities are decoupled because of $[\sigma^a\otimes\mathbb{1},\mathbb{1}\otimes\tau^\mu]=0$. However, the last commutation relation indicates that the spin and pseudospin dynamics are indeed entangled when taking into account local variations in the texture. This is due to the projection into the lowest LL, which yields the noncommutativity of the orbital degrees of freedom [Eq. (A4)]. It may also be seen directly from Eq. (A11): if we had $[f(\mathbf{q}),f(\mathbf{q}')]=0$, the anticommutator term $\sim\{A,B\}$ would vanish, and one would obtain $[\bar{S}^a(\mathbf{q}),\bar{P}^\mu(\mathbf{q}')]=0$. The same argument also yields the spin-charge and the pseudospin-charge entanglements, revealed by Eqs. (A7) and (A8).

Equation (A12) indicates that we generate, via the commutators, the generators $\sigma^a\otimes\tau^\mu$, which—together with $\sigma^a\otimes\mathbb{1}$ and $\mathbb{1}\otimes\tau^\mu$—give rise to the larger internal symmetry group SU(4), in which the SU(2)×SU(2) group, thus, needs to be embedded. The SU(N) extension of the magnetic-translation group, $\mathcal{T}_M\times$SU(N), with $N\geq 4$, was indeed the starting point of several other theoretical works on bilayer quantum Hall systems.[21,22,27,28] We have thus shown that a SU(4) description of the texture states is necessary even if the ground state has the reduced internal symmetry SU(2)×SU(2).

[1] S. M. Girvin, Phys. Today **53**(6), 39 (2000).
[2] X. G. Wen and A. Zee, Phys. Rev. Lett. **69**, 1811 (1992).
[3] Z. F. Ezawa and A. Iwazaki, Int. J. Mod. Phys. B **6**, 3205 (1992).
[4] A. H. MacDonald, P. M. Platzman, and G. S. Boebinger, Phys. Rev. Lett. **65**, 775 (1990).
[5] Luis Brey, Phys. Rev. Lett. **65**, 903 (1990).
[6] H. A. Fertig, Phys. Rev. B **40**, 1087 (1989).
[7] R. Côté, L. Brey, and A. H. MacDonald, Phys. Rev. B **46**, 10239 (1992).
[8] Tin-Lun Ho, Phys. Rev. Lett. **73**, 874 (1994).
[9] I. B. Spielman, J. P. Eisenstein, L. N. Pfeiffer, and K. W. West, Phys. Rev. Lett. **84**, 5808 (2000).
[10] K. Nomura and A. H. MacDonald, Phys. Rev. Lett. **96**, 256602 (2006).
[11] M. O. Goerbig, R. Moessner, and B. Douçot, Phys. Rev. B **74**, 161407(R) (2006).
[12] J. Alicea and M. P. A. Fisher, Phys. Rev. B **74**, 075422 (2006).
[13] T. H. R. Skyrme, Proc. R. Soc. London, Ser. A **260**, 127 (1961).
[14] S. L. Sondhi, A. Karlhede, S. A. Kivelson, and E. H. Rezayi, Phys. Rev. B **47**, 16419 (1993).
[15] S. E. Barrett, G. Dabbagh, L. N. Pfeiffer, K. W. West, and R. Tycko, Phys. Rev. Lett. **74**, 5112 (1995).
[16] For a review, see K. Moon, H. Mori, K. Yang, S. M. Girvin, A. H. MacDonald, L. Zheng, D. Yoshioka, and S. C. Zhang, Phys. Rev. B **51**, 5138 (1995); S. M. Girvin and A. H. MacDonald, in *Perspectives in Quantum Hall Effects*, edited by S. Das Sarma and A. Pinczuk (Wiley, New York, 1997).
[17] S. M. Girvin, in *Topological Aspects of Low-Dimensional Systems: Ecole d'Ete de Physique Théorique LXIX*, edited by A. Comptet, T. Jolicoeur, S. Ouvry, and F. David (Springer, New York, 1999).
[18] See, e.g., M. Rasolt, B. I. Halperin, and David Vanderbilt, Phys. Rev. Lett. **57**, 126 (1986).
[19] Y. P. Shkolnikov, S. Misra, N. C. Bishop, E. P. De Poortere, and M. Shayegan, Phys. Rev. Lett. **95**, 066809 (2005).
[20] For a review on graphene, see A. H. Castro Neto, F. Guinea, N. M. R. Peres, K. S. Novoselov, and A. K. Geim, arXiv:0709.1163, Rev. Mod. Phys. (to be published).
[21] Z. F. Ezawa, Phys. Rev. Lett. **82**, 3512 (1999); *Quantum Hall Effects: Field Theoretical Approach and Related Topics* (World Scientific, Singapore, 2000).
[22] D. P. Arovas, A. Karlhede, and D. Lilliehöök, Phys. Rev. B **59**, 13147 (1999).
[23] K. Yang, S. Das Sarma, and A. H. MacDonald, Phys. Rev. B **74**, 075423 (2006).
[24] R. Côté and A. H. MacDonald, Phys. Rev. B **44**, 8759 (1991).
[25] R. Côté, A. H. MacDonald, Luis Brey, H. A. Fertig, S. M. Girvin, and H. T. C. Stoof, Phys. Rev. Lett. **78**, 4825 (1997).
[26] Z. F. Ezawa and K. Hasebe, Phys. Rev. B **65**, 075311 (2002).
[27] Z. F. Ezawa, G. Tsitsishvili, and K. Hasebe, Phys. Rev. B **67**, 125314 (2003).
[28] Z. F. Ezawa and G. Tsitsishvili, Phys. Rev. B **70**, 125304 (2004).
[29] J. Bourassa, B. Roostaei, R. Côté, H. A. Fertig, and K. Mullen, Phys. Rev. B **74**, 195320 (2006).
[30] R. Côté, D. B. Boisvert, J. Bourassa, M. Boissonneault, and H. A. Fertig, Phys. Rev. B **76**, 125320 (2007).
[31] Schmidt decomposition, e.g., http://www.lkb.ens.fr/recherche/qedcav/college/2002/SHCdF2002-2.pdf
[32] I. B. Spielman, L. A. Tracy, J. P. Eisenstein, L. N. Pfeiffer, and K. W. West, Phys. Rev. Lett. **94**, 076803 (2005).
[33] N. Kumada, K. Muraki, K. Hashimoto, and Y. Hirayama, Phys. Rev. Lett. **94**, 096802 (2005).
[34] E. I. Rashba, L. E. Zhukov, and A. L. Efros, Phys. Rev. B **55**, 5306 (1997).
[35] A. A. Burkov and A. H. MacDonald, Phys. Rev. B **66**, 115320 (2002).
[36] N. D. Mermin, Rev. Mod. Phys. **51**, 591 (1979).
[37] D. A. Abanin, P. A. Lee, and L. S. Levitov, Phys. Rev. Lett. **98**, 156801 (2007).
[38] J.-N. Fuchs and P. Lederer, Phys. Rev. Lett. **98**, 016803 (2007).
[39] I. F. Herbut, Phys. Rev. B **75**, 165411 (2007); **76**, 085432 (2007).
[40] I. A. Luk'yanchuk and A. M. Bratkovsky, Phys. Rev. Lett. **100**, 176404 (2008).
[41] Y. Zhang, Z. Jiang, J. P. Small, M. S. Purewal, Y. W. Tan, M. Fazlollahi, J. D. Chudow, J. A. Jaszczak, H. L. Stormer, and P. Kim, Phys. Rev. Lett. **96**, 136806 (2006).
[42] A. Stern and B. I. Halperin, Phys. Rev. Lett. **88**, 106801 (2002).
[43] M. Kellogg, J. P. Eisenstein, L. N. Pfeiffer, and K. W. West, Phys. Rev. Lett. **93**, 036801 (2004); E. Tutuc, M. Shayegan, and D. A. Huse, *ibid.* **93**, 036802 (2004).

[44] J. Schliemann, S. M. Girvin, and A. H. MacDonald, Phys. Rev. Lett. **86**, 1849 (2001).
[45] P. Giudici, K. Muraki, N. Kumada, Y. Hirayama, and T. Fujisawa, Phys. Rev. Lett. **100**, 106803 (2008).
[46] B. I. Halperin, P. A. Lee, and N. Read, Phys. Rev. B **47**, 7312 (1993).
[47] S. H. Simon, E. H. Rezayi, and M. V. Milovanovic, Phys. Rev. Lett. **91**, 046803 (2003).
[48] G. Moller and S. H. Simon, Phys. Rev. B **77**, 075319 (2008).
[49] Z. Papić and M. V. Milovanović, Phys. Rev. B **75**, 195304 (2007).
[50] R. Rajaraman, *Solitons and Instantons* (North-Holland, Amsterdam, 1982).
[51] H. Fukuyama, Solid State Commun. **17**, 1323 (1975).
[52] D. J. Rowe, A. Ryman, and G. Rosensteel, Phys. Rev. A **22**, 2362 (1980).
[53] S. M. Girvin, A. H. MacDonald, and P. M. Platzman, Phys. Rev. B **33**, 2481 (1986).